JPE 18-1-16

https://doi.org/10.6113/JPE.2018.18.1.171
ISSN(Print): 1598-2092 / ISSN(Online): 2093-4718

Research on a Multi-Objective Control Strategy for Current-source PWM Rectifiers under Unbalanced and Harmonic Grid Voltage Conditions

Yi-Wen Geng*, Hai-Wei Liu*, Ren-Xiong Deng†, Fang-Fang Tian*, Hao-Feng Bai**, and Kai Wang*

*,†School of Electrical and Power Engineering, China University of Mining and Technology, Xuzhou, China
**Department of Energy Technology, Aalborg University, Aalborg, Denmark

Abstract

Unbalanced and distorted grid voltages cause the grid side current of a current source PWM rectifier to be heavily distorted. They can also cause the DC-link current to fluctuate with a huge amplitude. In order to enhance the performance of a current-source PWM rectifier under unbalanced and harmonic grid voltage conditions, a mathematical model of a current-source PWM rectifier is established and a flexible multi-objective control strategy is proposed to control the DC-link current and grid-current. The fundamental positive/negative sequence, 5th and 7th order harmonic components of the grid voltage are first separated with the proposed control strategy. The grid current reference are optimized based on three objectives: 1) sinusoidal and symmetrical grid current, 2) sinusoidal grid current and elimination of the DC-current 2nd order fluctuations, and 3) elimination of the DC-current 2nd and 6th order fluctuations. To avoid separation of the grid current components, a multi-frequency proportional-resonant controller is applied to control the fundamental positive/negative sequence, 5th and 7th order harmonic current. Finally, experimental results verify the effectiveness of proposed control strategy.

Key words: Current-source PWM rectifier, Proportional-resonant controller, Suppression for harmonic current, Unbalanced and harmonic grid voltage

I. INTRODUCTION

Pulse Width Modulation (PWM) rectifiers can be divided into Voltage Source Rectifiers (VSRs) and Current Source Rectifiers (CSRs). Due to its simpler structure, lower power consumption and easier control, the VSR has been the focus of a lot of research for PWM rectifiers. When compared with the VSR, the CSR also has gained some research attention in recent years due to its capability in terms of short-circuit protection, line current harmonic mitigation, input power factor regulation and direct current control. Due to above advantages, the CSR has been widely applied in active power filters [1], superconducting magnetic energy storage (SMES) [2], motor drives [3], [4], distributed generation systems [5], [6] and other occasions. With the development of SMES and power devices, the CSR will be applied more widely. In three-phase power systems, the randomness of electricity consumption, uneven distribution for single-phase loads and other factors lead to imbalances of the grid voltage [7]. The conventional control strategies of the PWM CSR under unbalanced grid voltage conditions cannot control the negative-sequence components. As a result, the DC-link current contains even order harmonics, and the grid-side current becomes unbalanced and distorted with odd order harmonics [8]. Therefore, a corresponding control strategy should be proposed to improve the system performance. In [9], the compensating current of the CSR reference under unbalanced grid voltages is calculated in the two-phase synchronously rotating frame. However, the grid current cannot be controlled by a closed-loop control strategy and the power factor is not adjustable. In order to control the positive/negative sequence current, the positive/negative sequence components of grid current are extracted in [10]. A

Manuscript received Apr. 26, 2017; accepted Sep. 24, 2017
Recommended for publication by Associate Editor Yijie Wang.
†Corresponding Author: renxiongdeng@163.com
Tel: +86-136-4520-5798, China University of Mining and Technology
*Sch. of Electrical and Power Eng., China Univ. Mining Tech., China
**Dept. of Energy Technology, Aalborg University, Denmark

Proportional Integral (PI) controller is adopted in the positive/negative sequence synchronously rotating reference frame. However, the control strategy still has some disadvantages, such as a complex three-loop control, a large number of parameters that need to be adjusted, and a more complex structure. Based on [10], the control structure is simplified in [11]. However, the controller still has to extract the positive/negative sequence components of the grid current, which introduces additional delays and affects the dynamic response of the system. To avoid the separation procedures between the positive and negative sequence components, a Proportional Integral Resonant (PIR) controller [12] and a Proportional Resonant (PR) controller [13] are adopted to control positive/negative sequence components of the VSR grid current. Control strategies under unbalanced grid voltages have been researched in [14]-[16]. However, these methods cannot be directly applied in CSRs for the following two reasons: (1) in terms of the CSR, there is large phase difference between the converter side current and the grid side current; (2) in terms of the converter side current of the CSR, when compared with L filter, the circuit with the LC filter is more likely to excite oscillations. Due to the above reasons, the control strategy of the CSR is more complicated under unbalanced voltage conditions.

In practice, in addition to three-phase unbalanced voltages, there also exist some harmonics in the grid voltage. In [17], the DC-side power fluctuations of a PWM rectifier are suppressed. However, the cause and expression of the power fluctuations are not given. In addition, the power fluctuations and grid current cannot be controlled coordinately. In [18], the 2nd order fluctuations of the DC-side power, and the 5th and 7th order harmonic fluctuations of the converter side current are all suppressed. However, the 6th order fluctuations of the DC-side power are not suppressed. Then, based on [18], an improved control method is proposed to reduce the input harmonic current or power ripple, and to enhance the operation performance of the PWM converter in [19]-[21]. The phases of the 6th pulsation caused by the 5th and 7th harmonic are different. However, they are superposed directly in these studies which introduce an error between the calculation and the measurement. In addition, the impact of unbalanced grid voltages is not considered in the control method. All of the control strategies in these studies are only proposed for VSRs, and not for CSRs. Furthermore, there is no control strategy proposed for a CSR under unbalanced and harmonic grid voltage conditions at present.

In this paper, a mathematical model of a current-source PWM rectifier under unbalanced and harmonic grid voltage conditions is established considering the fundamental negative sequence, and the 5th and 7th order harmonic components of the grid voltage in section II. Based on this model, a flexible multi-objective control strategy is proposed to control DC and AC currents in section III. For the proposed multi-objective control strategy, a multi-frequency proportional resonant controller is adopted to control the positive/negative sequence components of the grid side current. Simulations and experimental results verify the effectiveness of the proposed control strategy in sections IV and V. Finally, some conclusions are drawn in section VI.

II. Mathematical Model of a CSR under Unbalanced and Distorted Grid Voltage Conditions

A simplified system diagram of a three-phase CSR is shown in Fig. 1. In Fig. 1, e_a, e_b and e_c are the three-phase grid voltages; i_a, i_b and i_c represent the three-phase grid-side currents; i_{wa}, i_{wb} and i_{wc} represent the three-phase AC-side currents of the CSR; u_a, u_b and u_c represent the three-phase terminal voltages; i_{dc} represents the DC-link current; L represents the inductance for the AC side filter; C represents the capacitance for the AC side filter; L_{dc} represents the DC-link inductance; and R_{dc} represents the DC-link load.

Based on Fig. 1, the mathematical model in the two-phase stationary coordinate system is deduced as follows:

$$\begin{cases} L\dfrac{di_\alpha}{dt} = e_\alpha - u_\alpha - i_\alpha R \\ L\dfrac{di_\beta}{dt} = e_\beta - u_\beta - i_\beta R \end{cases} \tag{1}$$

$$\begin{cases} C\dfrac{du_\alpha}{dt} = i_\alpha - i_{w\alpha} \\ C\dfrac{du_\beta}{dt} = i_\beta - i_{w\beta} \end{cases} \tag{2}$$

Where, R represents the parasitic resistance of the AC line and inductance; e_α and e_β represent the components of the grid-side voltage in the two-phase stationary reference frame; u_α and u_β represent the terminal voltage in the two-phase stationary reference frame; i_α and i_β represent the components of the grid-side current in the two-phase stationary reference frame; and $i_{w\alpha}$ and $i_{w\beta}$ represent the current components of the AC side in the two-phase stationary reference frame.

For a three-phase CSR without a neutral line, when the grid voltage is unbalanced and contains the 5th and 7th order harmonics, the dq^+, dq^-, dq^{5-} and dq^{7+} reference vectors are shown in Fig. 2.

As shown in Fig. 2, the dq^+-axis is aligned with the positive sequence grid voltage vector rotating at the angular speed of ω, the dq^--axis is aligned with the negative sequence grid voltage vector rotating at the angular speed of $-\omega$, while for the dq^{5-} and dq^{7+} reference frames, as can be seen from Fig. 2, they rotate at angular speeds of -5ω and 7ω. In addition, ω is the fundamental frequency of grid voltage; and φ, θ and γ represent initial phase shifts for the negative sequence of the fundamental and harmonic components of -5ω and 7ω, respectively.

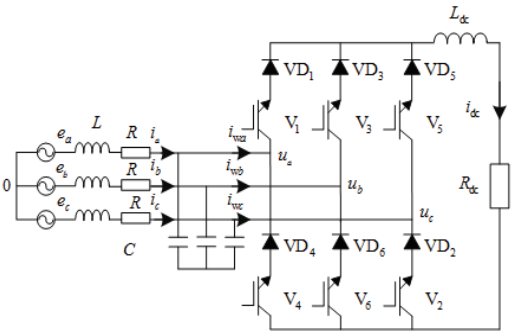

Fig. 1. System diagram of a three-phase CSR.

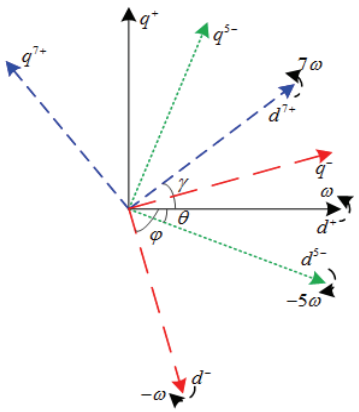

Fig. 2. Vector diagram of the dq^+, dq^-, dq^{5-} and dq^{7+} reference frames.

The apparent power $\boldsymbol{S}_{dq}$ can be expressed as follows:

$$\begin{aligned}\boldsymbol{S}_{dq} &= \frac{3}{2}\boldsymbol{E}\cdot\boldsymbol{I}^* \\ &= \frac{3}{2}\left(\boldsymbol{E}_{dq}^{+}e^{j\omega t}+\boldsymbol{E}_{dq}^{-}e^{-j\omega t}+\boldsymbol{E}_{5dq}^{-}e^{-5j\omega t}+\boldsymbol{E}_{7dq}^{+}e^{7j\omega t}\right)\cdot \\ &\left(\boldsymbol{I}_{dq}^{+}e^{j\omega t}+\boldsymbol{I}_{dq}^{-}e^{-j\omega t}+\boldsymbol{I}_{5dq}^{-}e^{-5j\omega t}+\boldsymbol{I}_{7dq}^{+}e^{7j\omega t}\right)^*\end{aligned} \tag{3}$$

Where, $\boldsymbol{E}_{dq}^{+}$, $\boldsymbol{E}_{dq}^{-}$, $\boldsymbol{E}_{dq}^{5-}$ and $\boldsymbol{E}_{dq}^{7+}$ represent the fundamental positive/negative sequence components, the 5th negative sequence and 7th positive sequence components of the grid voltage, respectively. $\boldsymbol{I}_{dq}^{+}$, $\boldsymbol{I}_{dq}^{-}$, $\boldsymbol{I}_{dq}^{5-}$ and $\boldsymbol{I}_{dq}^{7+}$ represent the fundamental positive/negative sequence components, the 5th negative sequence components and the 7th positive sequence components of the grid current, respectively.

The instantaneous active power and reactive power can be expressed as follows:

$$\begin{aligned}P(t)=&P_0+P_{c2}\cos\varphi+P_{s2}\sin\varphi+P_{5c6}\cos\theta+P_{5s6}\sin\theta+\\ &P_{7c6}\cos\gamma+P_{7s6}\sin\gamma+P_{c4}\cos(\varphi-\theta)+\\ &P_{s4}\sin(\varphi-\theta)+P_{c8}\cos(\varphi+\gamma)+P_{s8}\sin(\varphi+\gamma)+\\ &P_{c12}\cos(\theta+\gamma)+P_{s12}\sin(\theta+\gamma)\end{aligned} \tag{4}$$

$$\begin{aligned}Q(t)=&Q_0+Q_{c2}\cos\varphi+Q_{s2}\sin\varphi+Q_{5c6}\cos\theta+Q_{5s6}\sin\theta+\\ &Q_{7c6}\cos\gamma+Q_{7s6}\sin\gamma+Q_{c4}\cos(\varphi-\theta)+\\ &Q_{s4}\sin(\varphi-\theta)+Q_{c8}\cos(\varphi+\gamma)+Q_{s8}\sin(\varphi+\gamma)+\\ &Q_{c12}\cos(\theta+\gamma)+Q_{s12}\sin(\theta+\gamma)\end{aligned} \tag{5}$$

As represented in (4)-(5), the instantaneous output power contains some harmonic components under distorted grid voltage conditions. The average terms P_0 and Q_0 are the active and reactive powers which are given by (6)-(7). P_{c2}, P_{s2}, Q_{c2} and Q_{s2} represent the cosine and sine terms with the 2nd order component of the active and reactive powers, respectively, as shown in (8). In addition P_{c4}, P_{s4}, Q_{c4} and Q_{s4} represent the cosine and sine terms with the 4th order component of active and reactive powers, respectively, as shown in (9). P_{5c6}, P_{5s6}, Q_{5c6} and Q_{5s6} represent the cosine and sine terms with the 6th order component of the active and reactive powers that are caused by the 5th order harmonic, as shown in (10). Meanwhile, P_{7c6}, P_{7s6}, Q_{7c6} and Q_{7s6} represent the cosine and sine terms with the 6th order component of the active and reactive powers that are caused by the 7th order harmonic, as shown in (11). P_{c8}, P_{s8}, Q_{c8}, Q_{s8}, P_{c12}, P_{s12}, Q_{c12} and Q_{s12} represent the cosine and sine terms with the 8th and 12th order components of the active and reactive powers, respectively, as shown in (12)-(13).

$$\begin{aligned}P_0=&1.5\left(e_d^+i_d^++e_q^+i_q^++e_d^-i_d^-+e_q^-i_q^-\right)+\\ &1.5\left(e_{5d}^-i_{5d}^-+e_{5q}^-i_{5q}^-+e_{7d}^+i_{7d}^++e_{7q}^+i_{7q}^+\right)\end{aligned} \tag{6}$$

$$\begin{aligned}Q_0=&1.5\left(-e_d^+i_q^++e_q^+i_d^+-e_d^-i_q^-+e_q^-i_d^-\right)+\\ &1.5\left(-e_{5d}^-i_{5q}^-+e_{5q}^-i_{5d}^--e_{7d}^+i_{7q}^++e_{7q}^+i_{7d}^+\right)\end{aligned} \tag{7}$$

$$\begin{bmatrix}P_{c2}\\P_{s2}\\Q_{c2}\\Q_{s2}\end{bmatrix}=1.5\begin{bmatrix}e_d^- & e_q^- & e_d^+ & e_q^+\\ e_q^- & -e_d^- & -e_q^+ & e_d^+\\ e_q^- & -e_d^- & e_q^+ & -e_d^+\\ -e_d^- & -e_q^- & e_d^+ & e_q^+\end{bmatrix}\begin{bmatrix}i_d^+\\i_q^+\\i_d^-\\i_q^-\end{bmatrix} \tag{8}$$

$$\begin{bmatrix}P_{c4}\\P_{s4}\\Q_{c4}\\Q_{s4}\end{bmatrix}=1.5\begin{bmatrix}e_{5d}^- & e_{5q}^- & e_d^- & e_q^-\\ e_{5q}^- & e_{5d}^- & e_q^- & -e_d^-\\ e_{5q}^- & -e_{5d}^- & e_q^- & -e_d^-\\ e_{5d}^- & e_{5q}^- & -e_d^- & -e_q^-\end{bmatrix}\begin{bmatrix}i_d^-\\i_q^-\\i_{5d}^-\\i_{5q}^-\end{bmatrix} \tag{9}$$

$$\begin{bmatrix}P_{5c6}\\P_{5s6}\\Q_{5c6}\\Q_{5s6}\end{bmatrix}=1.5\begin{bmatrix}e_{5d}^- & e_{5q}^- & e_d^+ & e_q^+\\ e_{5q}^- & -e_{5d}^- & -e_q^+ & e_d^+\\ e_{5q}^- & -e_{5d}^- & e_q^+ & -e_d^+\\ -e_{5d}^- & -e_{5q}^- & e_d^+ & e_q^+\end{bmatrix}\begin{bmatrix}i_d^+\\i_q^+\\i_{5d}^-\\i_{5q}^-\end{bmatrix} \tag{10}$$

$$\begin{bmatrix}P_{7c6}\\P_{7s6}\\Q_{7c6}\\Q_{7s6}\end{bmatrix}=1.5\begin{bmatrix}e_{7d}^+ & e_{7q}^+ & e_d^+ & e_q^+\\ -e_{7q}^+ & e_{7d}^+ & e_q^+ & -e_d^+\\ e_{7q}^+ & -e_{7d}^+ & e_q^+ & -e_d^+\\ e_{7d}^+ & e_{7q}^+ & -e_d^+ & -e_q^+\end{bmatrix}\begin{bmatrix}i_d^+\\i_q^+\\i_{7d}^+\\i_{7q}^+\end{bmatrix} \tag{11}$$

$$\begin{bmatrix} P_{c8} \\ P_{s8} \\ Q_{c8} \\ Q_{s8} \end{bmatrix} = 1.5 \begin{bmatrix} e_{7d}^{+} & e_{7q}^{+} & e_{d}^{-} & e_{q}^{-} \\ e_{7q}^{+} & e_{7d}^{+} & e_{q}^{-} & e_{d}^{-} \\ e_{7q}^{+} & -e_{7d}^{+} & e_{q}^{-} & -e_{d}^{-} \\ e_{7d}^{+} & e_{7q}^{+} & -e_{d}^{-} & -e_{q}^{-} \end{bmatrix} \begin{bmatrix} i_{d}^{-} \\ i_{q}^{-} \\ i_{7d}^{+} \\ i_{7q}^{+} \end{bmatrix} \tag{12}$$

$$\begin{bmatrix} P_{c12} \\ P_{s12} \\ Q_{c12} \\ Q_{s12} \end{bmatrix} = 1.5 \begin{bmatrix} e_{7d}^{+} & e_{7q}^{+} & e_{5d}^{-} & e_{5q}^{-} \\ -e_{7q}^{+} & e_{7d}^{+} & e_{5q}^{-} & -e_{5d}^{-} \\ e_{7q}^{+} & -e_{7d}^{+} & e_{5q}^{-} & -e_{5d}^{-} \\ e_{7d}^{+} & e_{7q}^{+} & -e_{5d}^{-} & -e_{5q}^{-} \end{bmatrix} \begin{bmatrix} i_{5d}^{-} \\ i_{5q}^{-} \\ i_{7d}^{+} \\ i_{7q}^{+} \end{bmatrix} \tag{13}$$

It is worth noting that the 2nd and 6th order components are only introduced by the interactions between the fundamental positive/negative sequence components and the harmonic components of the grid voltage or current. In addition, the 4th, 8th and 12th order components are only caused by the interactions among the fundamental, 5th and 7th order harmonic components of the grid voltages and grid currents. As a result, the 4th, 8th and 12th order harmonics, which behave less significantly when compared with the 2nd and 6th order harmonics, can be ignored in the system control design.

III. Control Strategy for a CSR under Unbalanced and Distorted Grid Voltage Conditions

A. Extraction Method of Unbalanced and Distorted Voltage Components

The extraction of the fundamental positive/negative sequence and harmonic voltage components is the premise of the proposed control method. Since all of the components of grid voltage cannot be separated by the conventional second-order generalized integrator (SOGI), the multiple second-order generalized integrator (MSOGI) technique is adopted in the paper [22].

When the grid voltage is unbalanced, the positive sequence voltage component in the two-phase stationary reference frame can be expressed as follows:

$$\boldsymbol{E}_{\alpha\beta}^{+} = \frac{1}{2}\begin{bmatrix} 1 & -q \\ q & 1 \end{bmatrix} \boldsymbol{E}_{\alpha\beta} \tag{14}$$

Similarly, the negative sequence component can be expressed by:

$$\boldsymbol{E}_{\alpha\beta}^{-} = \frac{1}{2}\begin{bmatrix} 1 & q \\ -q & 1 \end{bmatrix} \boldsymbol{E}_{\alpha\beta} \tag{15}$$

where, $\boldsymbol{E}_{\alpha\beta}$ represents the voltage vector in the α-β reference frame; $\boldsymbol{E}_{\alpha\beta}^{+}$ and $\boldsymbol{E}_{\alpha\beta}^{-}$ represent the positive/negative sequence voltage vectors in the α-β reference frame respectively; q is a 90 degree lagging phase-shifting operator.

According to (14) and (15), the conventional double second-order generalized integrator (DSOGI) can be introduced to obtain positive/negative sequence components in the α-β reference frame.

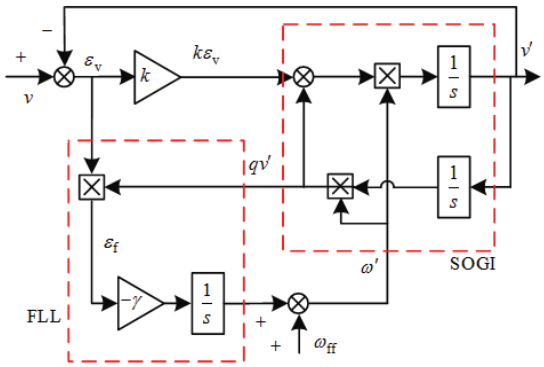

Fig. 3. Diagram of a second order generalized integrator quadrature single generator.

The second-order generalized integrator resting on a frequency locked loop (SOGI-FLL) is frequency adaptive. Its schematic diagram is shown in Fig. 3. In addition, the frequency locked loop (FLL) is capable of tracking the fundamental frequency of the system. As shown in Fig. 3, the input signal of the SOGI-FLL is v, and the output signals are the fundamental components of v, which is denoted as v' and its quadrature signal is qv'. Orthogonalization is achieved by the SOGI for quadrature-signals generation.

The transfer functions are expressed as follows:

$$D(s) = \frac{v'}{v}(s) = \frac{k\omega' s}{s^2 + k\omega' s + \omega'^2} \tag{16}$$

$$Q(s) = \frac{qv'}{v}(s) = \frac{k\omega'^2}{s^2 + k\omega' s + \omega'^2} \tag{17}$$

The amplitudes of $D(s)$ and $Q(s)$ at ω' are both unit. In addition, $Q(s)$ is 90-degrees lagged from $D(s)$. If the FLL is capable of tracking the frequency accurately, v' becomes the same as v, and the qv' output is 90 degrees lagged from the v' output, which is independent of the other parameters.

The quadrature-signals of the fundamental components in the α-axis and β-axis are obtained by the DSOGI. Then, the positive/negative sequence components of the grid voltage in the α-β coordinate system are obtained by the positive/negative sequence calculation (PNSC) block given in (14) and (15).

When the grid voltage contains the 5th and 7th order harmonics, the output of the conventional DSOGI is significantly distorted. Meanwhile, the 5th and 7th order components of the grid voltage cannot be separated by the DSOGI. Cross feedback SOGIs are adopted to detect the harmonic components of the grid voltage under unbalanced and harmonic grid voltage conditions [22]. The extraction method is called the multiple second-order generalized integrator FLL (MSOGI-FLL), as shown in Fig. 4.

As can be seen from Fig. 4, the MSOGI-FLL consists of 3 individual DSOGI-QSGs working in collaboration by using a cross feedback network. The inputs of the FLLs are provided by DSOGI-QSG-1, which is tuned at the fundamental frequency. In addition, the tuning frequencies of DSOGI-

QSG-5 and DSOGI-QSG-7 are set by 5 times and 7 times the fundamental frequency detected by the FLL. Furthermore, the input for each of the DSOGI-QSGs is the error between the original signal v and the other output of DSOGI-QSGs, which filtered out the other components detected by the rest of the DSOGI-QSGs.

As shown in Fig. 4, the output of SOGI-QSG-1, SOGI-QSG-5 and SOGI-QSG-7 are:

$$v'_{\alpha\beta} = D_1(s)\left(v_{\alpha\beta} - v'_{5\alpha\beta} - v'_{7\alpha\beta}\right) \tag{18}$$

$$v'_{5\alpha\beta} = D_5(s)\left(v_{\alpha\beta} - v'_{\alpha\beta} - v'_{7\alpha\beta}\right) \tag{19}$$

$$v'_{7\alpha\beta} = D_7(s)\left(v_{\alpha\beta} - v'_{\alpha\beta} - v'_{5\alpha\beta}\right) \tag{20}$$

Where:

$$D_1(s) = \frac{k\omega' s}{s^2 + k\omega' s + (\omega')^2} \tag{21}$$

$$D_5(s) = \frac{5k\omega' s}{s^2 + 5k\omega' s + (5\omega')^2} \tag{22}$$

$$D_7(s) = \frac{7k\omega' s}{s^2 + 7k\omega' s + (7\omega')^2} \tag{23}$$

According to (18) - (20):

$$v'_{\alpha\beta} = D_1(s)\frac{1 - D_5(s)}{1 - D_1(s)D_5(s)}\frac{1 - D_7(s)}{1 - D_1(s)D_7(s)}v_{\alpha\beta} \tag{24}$$

$$v'_{5\alpha\beta} = D_5(s)\frac{1 - D(s)}{1 - D_5(s)D(s)}\frac{1 - D_7(s)}{1 - D_5(s)D_7(s)}v_{\alpha\beta} \tag{25}$$

$$v'_{7\alpha\beta} = D_7(s)\frac{1 - D_1(s)}{1 - D_7(s)D_1(s)}\frac{1 - D_5(s)}{1 - D_7(s)D_5(s)}v_{\alpha\beta} \tag{26}$$

According to (24)-(26), bode diagrams of a MSOGI-FLL are shown in Fig. 5. Taking the 5th order component as an example, as can be seen in Fig. 5(b), (25) does not suppress the 5th order harmonic. However, it has a notch on the fundamental and the 7th order harmonic. Furthermore, the conventional DSOGI has no obvious effect on the fundamental

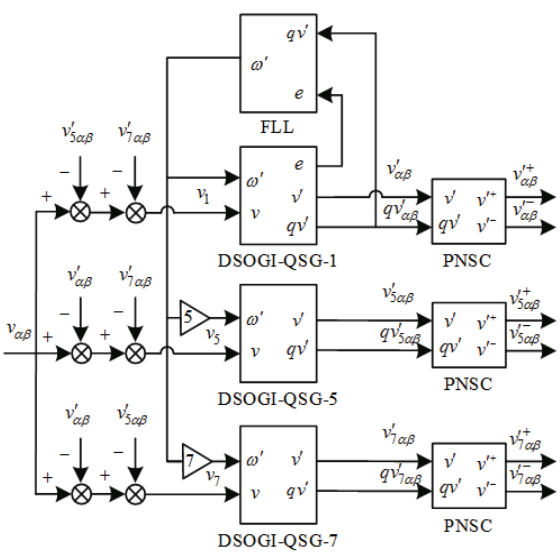

Fig. 4. Block diagram of a MSOGI-FLL.

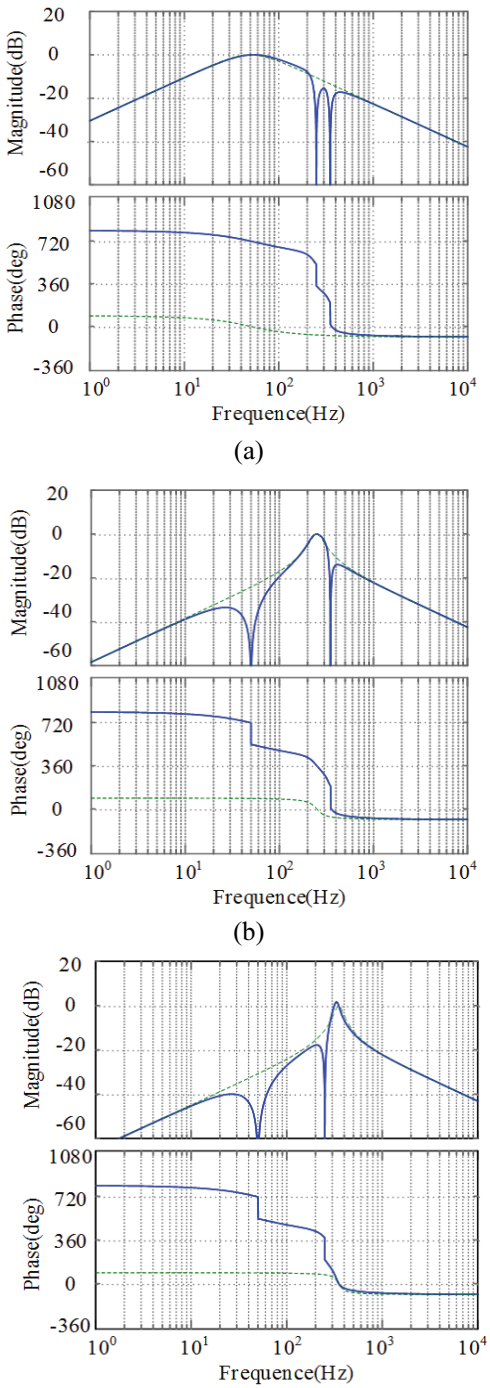

Fig. 5. Bode diagrams of a MSOGI-FLL: (a) Bode diagram of DSOGI-QSG-1; (b) Bode diagram of DSOGI-QSG-5; (c) Bode diagram of DSOGI-QSG-7.

or the 7th order harmonic. Similarly, the MSOGI-FLL also has a notch at the other frequencies, as shown in Fig. 5(a) and Fig. 5(c). As a result, under unbalanced and harmonic grid voltage conditions, the selective filtering characteristic for each of the DSOGI-QSGs is improved and its response is enhanced when compared with the dashed line, which represent bode diagrams of conventional DSOGI-QSG in Fig. 5.

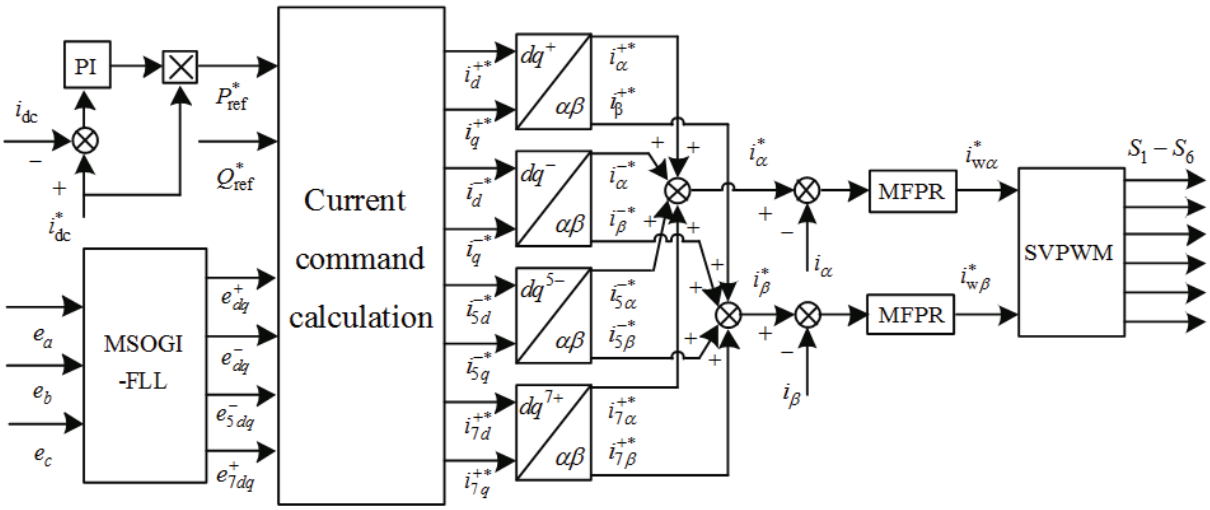

Fig. 6. Control structure of a CSR under unbalanced and harmonic voltage conditions.

B. Control Strategy

Under unbalanced and harmonic grid voltage conditions, the negative sequence, and 5th and 7th order harmonic components of the grid voltage lead to imbalance and distortion for the grid side current. These harmonic components result in fluctuations of the DC-link current, which causes the 2nd and 6th and to a lesser extent the 4th, 8th and 12th order harmonics. In addition, the DC-link current and instantaneous power fluctuate, which can lead to a malfunction of the grid protection device, or even damage to the rectifier. Therefore, an improved control strategy should be proposed to reduce the distortion and imbalance of the grid current as well as fluctuations of the DC-link current.

A schematic of the proposed control strategy is shown in Fig. 6. As can be seen, the PI controller is adopted in the outer current loop. It can also be seen that its output works as the reference of the DC voltage. Firstly, the voltage reference is multiplied by the DC-link current reference to obtain the active power reference P^*_{ref}. Then, the active power reference P^*_{ref}, reactive power reference Q^*_{ref} and each component of the grid voltage are directly transformed into the calculation module of the current reference. Its outputs are reference signals of the fundamental positive/negative sequence as well as the 5th and 7th order components of the grid current. Secondly, the error between the grid current reference and the grid current in the two-phase stationary reference frame is fed to the multi-frequency proportional-resonant (MFPR) controller of the inner loop. Finally, PWM signals are generated for the IGBTs in the bridge of the inverter.

A block diagram and bode diagram of the MFPR controller are shown in Fig. 7. In Fig. 7(a), ω_0, ω_c and K_p represent the fundamental frequency, cut-off frequency and scale parameter of the grid voltage, respectively. K_{I1}、K_{I5} and K_{I7} represent integral parameters at the fundamental, 5th and 7th order frequency, respectively. As shown in Fig. 7(b), the Gain of the MFPR at ω_0, $5\omega_0$ and $7\omega_0$ is extremely high when compared with the other frequencies. Thus, the MFPR can track the fundamental frequency as well as the 5th and 7th order harmonic signals with negligible error. It can also control the 5th and 7th order harmonic components.

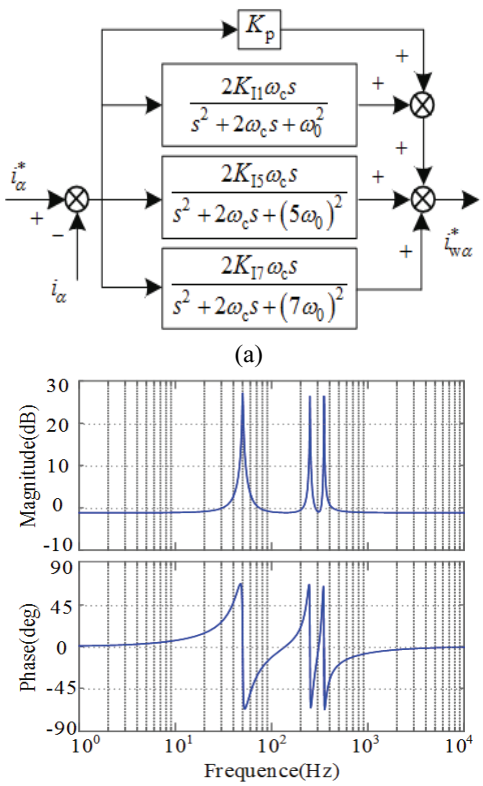

Fig. 7. MFPR controller with 5th and 7th harmonic compensation: (a) block diagram of a MFPR; (b) bode diagram of a MFPR.

When the grid voltage is unbalanced and contains the 5th and 7th order harmonics, the grid voltage is multiplied by the

fundamental positive sequence components of the grid current to obtain power. Due to the existence of negative sequence as well as the 5th and 7th order harmonic components, the power contains 2nd and 6th order fluctuations, leading to 2nd and 6th order fluctuations of the DC-link current. Therefore, in order to eliminate the 2nd and 6th order fluctuations of the DC-link current, the grid current has to contain some negative sequence and harmonic components. In addition, there is a tradeoff between the elimination of imbalance, distortion of the grid current and suppression of DC-current fluctuations. Therefore, for different control objects, the corresponding references of the grid current must be calculated.

There are three specific objectives shown in the following part:

1) Obtaining a Sinusoidal, Symmetrical Grid Current

This objective can be launched when there are no demands in terms of the quality of the DC current under unbalanced and harmonic grid voltage conditions, such as electric smelting, which does not have a bad influence on the grid while satisfying the application. To ensure that the grid current is sinusoidal and symmetrical, the reference values of the fundamental negative sequence as well as the 5th and 7th order components should be set to zero. Substituting (6) into (7) yields:

$$\begin{cases} i_d^{+*}=\dfrac{2}{3}\times\dfrac{P_{g0}^*}{e_d^+} \\ i_q^{+*}=-\dfrac{2}{3}\dfrac{Q_{g0}^*}{e_d^+} \end{cases} \quad \begin{cases} i_d^{-*}=0 \\ i_q^{-*}=0 \end{cases} \quad \begin{cases} i_{5d}^{-*}=0 \\ i_{5q}^{-*}=0 \end{cases} \quad \begin{cases} i_{7d}^{+*}=0 \\ i_{7q}^{+*}=0 \end{cases} \tag{27}$$

2) Obtaining a Sinusoidal Grid Current and Eliminating the 2nd Order Fluctuations of the DC-link Current

This objective can be launched when there are low demands in terms of the quality of the DC current under unbalanced and harmonic grid voltage conditions, such as motor drivers. In order to eliminate the 2nd order harmonic of the DC-link current, the harmonic current can be regulated to achieve the control objectives with the constant DC-link current, by ensuring that:

$$\begin{cases} P_{c2}^*=0 \\ P_{s2}^*=0 \end{cases} \tag{28}$$

Substituting (28) into (8) yields:

$$\begin{bmatrix} i_d^{+*} \\ i_q^{+*} \\ i_d^{-*} \\ i_q^{-*} \end{bmatrix}=\frac{2}{3}\begin{bmatrix} e_d^+ & e_q^+ & e_d^- & e_q^- \\ e_q^+ & -e_d^+ & e_q^- & -e_d^- \\ e_d^- & e_q^- & e_d^+ & e_q^+ \\ e_q^- & -e_d^- & -e_q^+ & e_d^+ \end{bmatrix}^{-1}\begin{bmatrix} P_0^* \\ Q_0^* \\ 0 \\ 0 \end{bmatrix} \tag{29}$$

According to (29), the reference values of the fundamental positive/negative sequence current are calculated as follows:

$$\begin{cases} i_d^{+*}=\dfrac{2}{3}\times\dfrac{e_d^+P_{g0}^*}{\left(e_d^+\right)^2-\left(e_d^-\right)^2-\left(e_q^-\right)^2} \\ i_q^{+*}=\dfrac{2}{3}\times\dfrac{-e_d^+Q_{g0}^*}{\left(e_d^+\right)^2+\left(e_d^-\right)^2+\left(e_q^-\right)^2} \\ i_d^{-*}=-\dfrac{e_d^-}{e_d^+}i_d^+-\dfrac{e_q^-}{e_d^+}i_q^+ \\ i_q^{-*}=\dfrac{e_d^-}{e_d^+}i_q^+-\dfrac{e_q^-}{e_d^+}i_d^+ \end{cases} \tag{30}$$

Coincidentally, according to (27), to ensure a sinusoidal grid current, the reference values of the 5th and 7th order components for the grid current should be set to zero, which is shown in (31).

$$\begin{cases} i_{5d}^{-*}=0 \\ i_{5q}^{-*}=0 \end{cases} \quad \begin{cases} i_{7d}^{+*}=0 \\ i_{7q}^{+*}=0 \end{cases} \tag{31}$$

3) Eliminating the 2nd and 6th Order Harmonics of the DC-link Current

This objective can be launched when the demand in terms of the quality of the DC current is extremely high under unbalanced and harmonic grid voltage conditions, such as precise instruments and medical equipment. In order to eliminate the 2nd and 6th order harmonic of the DC-link current, the harmonic currents can be regulated to achieve the control objective with the constant DC-link current, by ensuring that:

$$\begin{cases} P_{c2}^*=0 \\ P_{s2}^*=0 \end{cases} \quad \begin{cases} P_{5c6}^*=0 \\ P_{5s6}^*=0 \end{cases} \quad \begin{cases} P_{7c6}^*=0 \\ P_{7s6}^*=0 \end{cases} \tag{32}$$

Substituting (32) into (8), (10) and (11) yields:

$$\begin{bmatrix} i_d^+ \\ i_q^+ \\ i_d^- \\ i_q^- \\ i_{5d}^- \\ i_{5q}^- \\ i_{7d}^+ \\ i_{7q}^+ \end{bmatrix}=\frac{2}{3}\begin{bmatrix} e_d^+ & e_q^+ & e_d^- & e_q^- & e_{5d}^- & e_{5q}^- & e_{7d}^+ & e_{7q}^+ \\ e_q^+ & -e_d^+ & e_q^- & -e_d^- & e_{5q}^- & -e_{5d}^- & e_{7q}^+ & -e_{7d}^+ \\ e_d^- & e_q^- & e_d^+ & e_q^+ & 0 & 0 & 0 & 0 \\ e_q^- & -e_d^- & -e_q^+ & e_d^+ & 0 & 0 & 0 & 0 \\ e_{5d}^- & e_{5q}^- & 0 & 0 & e_d^+ & e_q^+ & 0 & 0 \\ e_{5q}^- & -e_{5d}^- & 0 & 0 & -e_q^+ & e_d^+ & 0 & 0 \\ e_{7d}^+ & e_{7q}^+ & 0 & 0 & 0 & 0 & e_d^+ & e_q^+ \\ -e_{7q}^+ & e_{7d}^+ & 0 & 0 & 0 & 0 & e_q^+ & -e_d^+ \end{bmatrix}^{-1}\begin{bmatrix} P_0^* \\ Q_0^* \\ 0 \\ 0 \\ 0 \\ 0 \\ 0 \\ 0 \end{bmatrix} \tag{33}$$

$$\begin{cases} i_d^{+*}=\dfrac{2}{3}\times\dfrac{e_d^+P_{g0}^*}{A} \\ i_q^{+*}=\dfrac{2}{3}\times\dfrac{-e_d^+Q_{g0}^*}{B} \end{cases} \quad \begin{cases} i_d^{-*}=-\dfrac{e_d^-}{e_d^+}i_d^{+*}-\dfrac{e_q^-}{e_d^+}i_q^{+*} \\ i_q^{-*}=\dfrac{e_d^-}{e_d^+}i_q^{+*}-\dfrac{e_q^-}{e_d^+}i_d^{+*} \end{cases}$$

$$\begin{cases} i_{5d}^{-*}=-\dfrac{e_{5d}^-}{e_d^+}i_d^{+*}-\dfrac{e_{5q}^-}{e_d^+}i_q^{+*} \\ i_{5q}^{-*}=-\dfrac{e_{5q}^-}{e_d^+}i_d^{+*}+\dfrac{e_{5d}^-}{e_d^+}i_q^{+*} \end{cases} \quad \begin{cases} i_{7d}^{+*}=-\dfrac{e_{7d}^+}{e_d^+}i_d^{+*}-\dfrac{e_{7q}^+}{e_d^+}i_q^{+*} \\ i_{7q}^{+*}=-\dfrac{e_{7q}^+}{e_d^+}i_d^{+*}+\dfrac{e_{7d}^+}{e_d^+}i_q^{+*} \end{cases} \tag{34}$$

$$\begin{cases} A=\left(e_d^+\right)^2-\left(e_d^-\right)^2-\left(e_q^-\right)^2-\left(e_{5d}^-\right)^2-\left(e_{5q}^-\right)^2-\left(e_{7d}^+\right)^2-\left(e_{7q}^+\right)^2 \\ B=\left(e_d^+\right)^2+\left(e_d^-\right)^2+\left(e_q^-\right)^2+\left(e_{5d}^-\right)^2+\left(e_{5q}^-\right)^2+\left(e_{7d}^+\right)^2+\left(e_{7q}^+\right)^2 \end{cases}$$

TABLE I
EXPERIMENT PARAMETERS

Rated source voltage	60V
Grid voltage frequency	50Hz
AC-link inductance	3mH
AC-link capacitance	50μF
DC-link current	10A
DC-link inductance	12mH
DC-link load resistance	3Ω
PWM frequency	5kHz

According to (33), the reference values of the fundamental positive/negative sequence as well as the 5th and 7th order components can be calculated as shown in (34).

IV. SIMULATION RESULTS

In order to verify the effectiveness of the proposed control strategy, simulations are carried out based on the MATLAB/Simulink platform. The parameters of the CSR system are shown in TABLE I. Both the 5^{th} and 7^{th} order harmonic component contents of the grid voltage are set at 10% throughout the entire simulation. In addition, the imbalance degree of the grid voltage is set at 10%. The resulting grid voltage waveform is shown in Fig. 8.

Under unbalanced and harmonic grid voltage conditions, the conventional control strategy is adopted in the CSR system. However, the conventional single PI current control scheme is not capable of effectively controlling the fundamental negative-sequence or the 5^{th} and 7^{th} order currents. Its simulation results are shown in Fig. 9. In Fig. 9, the grid current is unbalanced and harmonically distorted. In addition, the total harmonic distortion (THD) is 18.57% and the dc-link current contains pulsations at frequencies of 6ω and 2ω. Furthermore, the fluctuation is ± 0.4A, which is consistent with the mathematical expression derived above.

The proposed improved control with objective 1 is employed to obtain a sinusoidal, symmetrical grid-side current. The grid current and DC-link current are shown in Fig. 10. When compared with the conventional control strategy, the grid-side current is more symmetrical and the harmonic component is effectively suppressed. The THD is 2.81%. However, 2^{nd} and 6^{th} order fluctuations of the DC-link current still exist. In addition, its magnitude is ± 0.4A. The grid voltage is unbalanced and distorted, which results in fluctuations of the dc-link current. As a result, the fluctuation is consistent with the theory. Therefore, objective 1 is achieved.

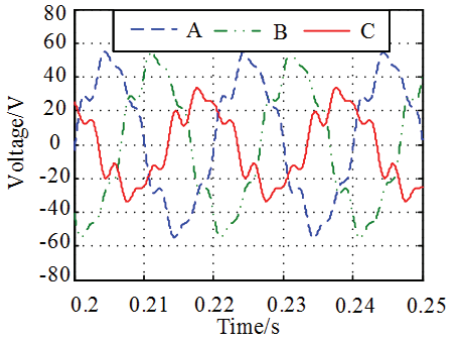

Fig. 8. Three-phase grid voltage under unbalanced and harmonic conditions.

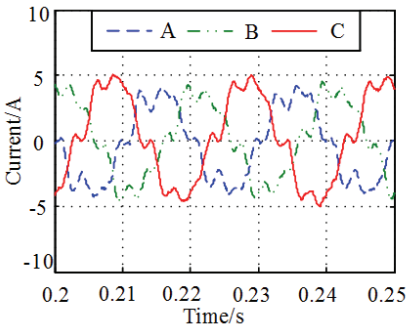

(a)

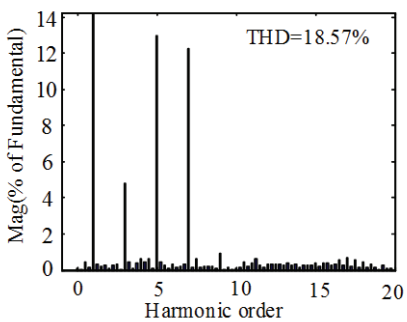

(b)

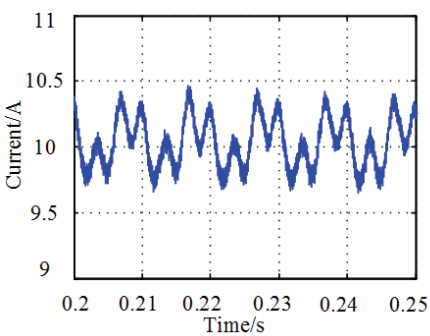

(c)

Fig. 9. Simulation waveforms of the conventional method: (a) grid current; (b) spectrum diagram of the grid current; (c) DC-link current.

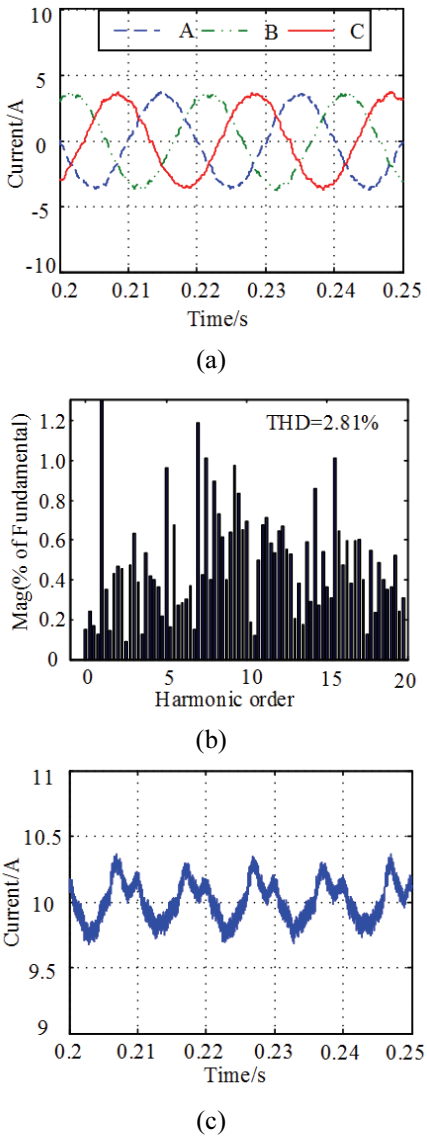

Fig. 10. Simulation waveforms of objective 1: (a) grid current; (b) spectrum diagram of the grid current; (c) DC-link current.

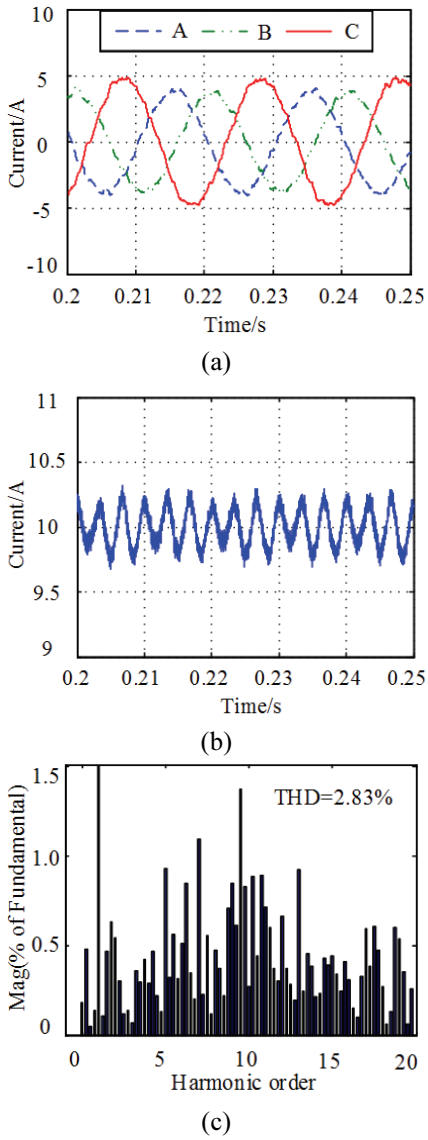

Fig. 11. Simulation waveforms of objective 2: (a) grid current; (b) spectrum diagram of the grid current; (c) DC-link current.

The proposed improved control with objective 2 is employed to obtain a sinusoidal grid-side current and to eliminate the 2nd order fluctuation of the DC-link current, as shown in Fig. 11. When compared with the conventional control strategy, the fluctuation of the DC-link current is suppressed to ± 0.3A. However, the 6th order fluctuations still exist. The THD is 2.83%. In addition, the negative-sequence components of the grid current are used to suppress the 2nd order fluctuations. Therefore, the increase of the imbalance degree is consistent with the theory. Therefore, objective 2 is achieved.

The proposed improved control with objective 3 is employed to eliminate the 2nd and 6th order fluctuation of the DC-link current, as shown in Fig. 12. When compared with the conventional control, the fluctuation of the DC-link current is suppressed to ± 0.1A, and the 2nd and 6th order fluctuations of the DC-link current are effectively suppressed. In addition, the THD is 15.16%. The negative-sequence components of the grid current are used to suppress the 2nd and 6th order fluctuations of the DC-link current. Thus, the increases of the imbalance degree and distortion are consistent with the theory. Therefore, objective 3 is achieved.

V. Experimental Results

In order to further verify the effectiveness of the proposed control strategy, an experimental platform was built, as shown in Fig. 13. The platform uses a TMS320F28335 as its controller and a PVS7010T AC source to provide grid voltage. Both the 5th and 7th order harmonic component contents of the grid voltage are set at 10% throughout the entire experiment. In addition, the imbalance degree of the

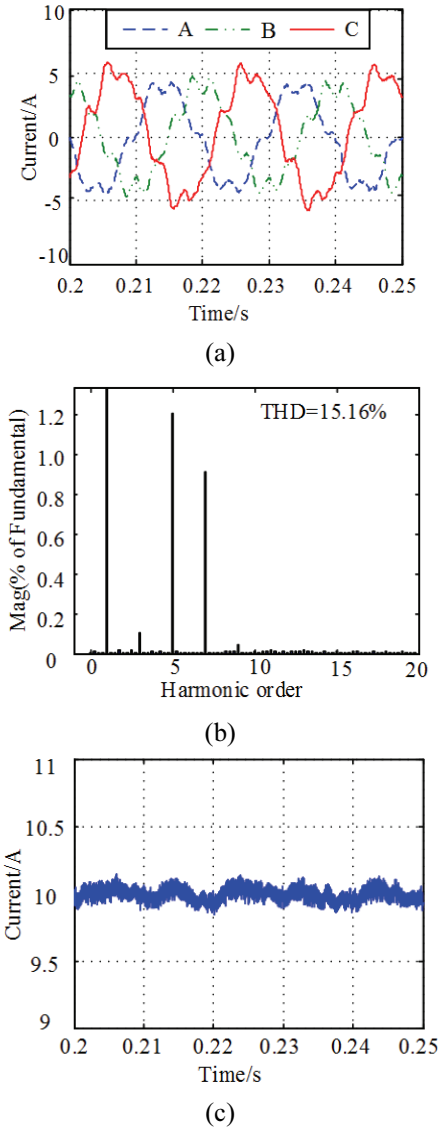

Fig. 12. Simulation waveforms of objective 3: (a) grid current; (b) spectrum diagram of the grid current; (c) DC-link current.

grid voltage is set at 10%. The grid voltage waveform is shown in Fig. 14. The parameters of the CSR system are the same as those of simulation as shown in TABLE I.

The experimental results are consistent with the simulation results. Experimental waveforms of the conventional method and the proposed control strategy are shown in Figs. 14-18.

As shown in Fig. 15, when the conventional method is employed, the grid current is unbalanced and harmonically distorted. The total harmonic distortion (THD) is 17.1% and the dc-link current contains pulsations at frequencies of 6ω and 2ω. In addition, the fluctuation is ± 0.5A.

When the proposed improved control with objective 1 is employed, the THD is 2.7%, and the magnitude of the 2nd and 6th order fluctuations of the DC-link current is ± 0.7A, as shown in Fig. 16. The grid voltage is unbalanced and distorted, resulting in fluctuations of the dc-link current.

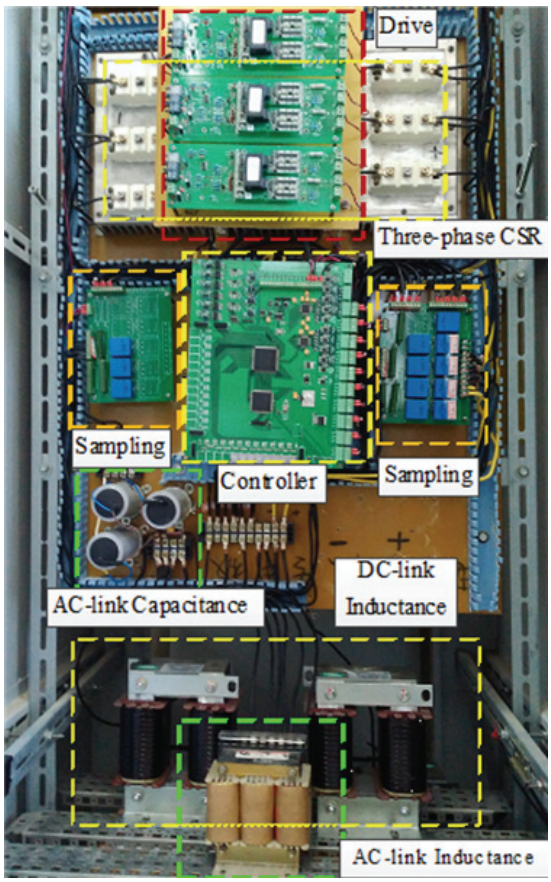

Fig. 13. Hardware prototype of a three-phase CSR.

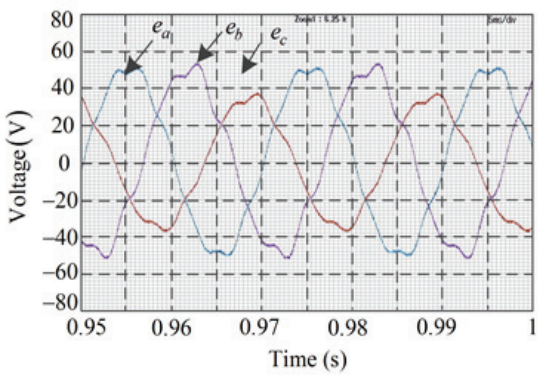

Fig. 14. Three-phase grid voltage under unbalanced and harmonic conditions.

Therefore, the fluctuation is consistent with the theory and the simulation results.

When the proposed improved control with objective 2 is employed, as shown in Fig. 17, the fluctuation of the DC-link current is suppressed to ± 0.4A. However, the 6th order fluctuations still exist. The THD is 2.6% and the imbalance degree is 6.5%. In addition, the negative sequence components of the grid current are used to suppress the 2nd order fluctuations. Thus, the increase of the imbalance degree is consistent with the theory and the simulation results.

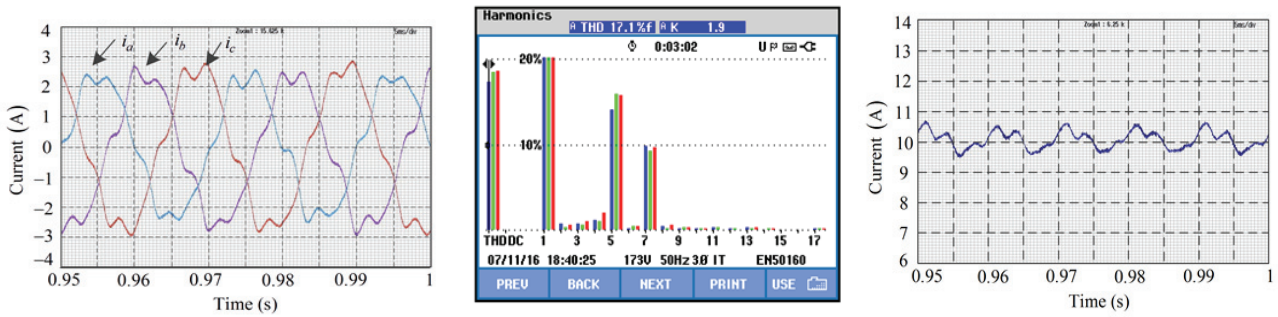

(a) (b) (c)

Fig. 15. Experimental waveforms of the conventional method: (a) grid current; (b) spectrum diagram of the grid current; (c) DC-link current.

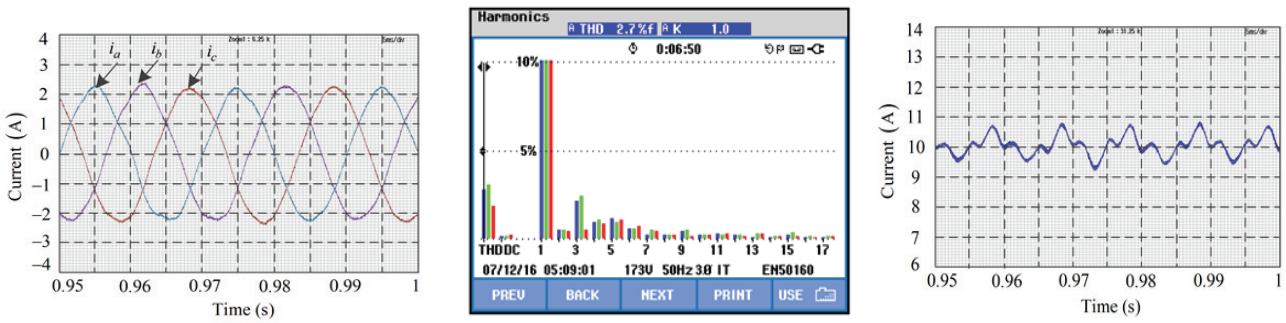

(a) (b) (c)

Fig. 16. Experimental waveforms of objective 1: (a) grid current; (b) spectrum diagram of the grid current; (c) DC-link current.

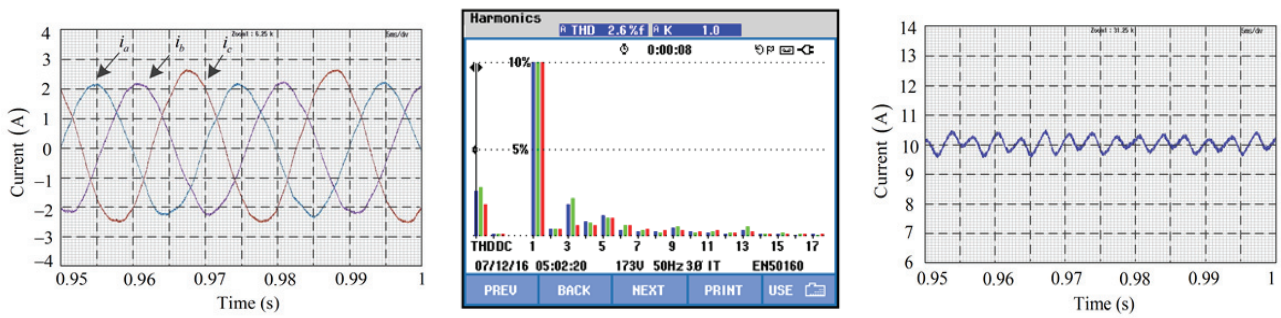

(a) (b) (c)

Fig. 17. Experimental waveforms of objective 2: (a) grid current; (b) spectrum diagram of the grid current; (c) DC-link current.

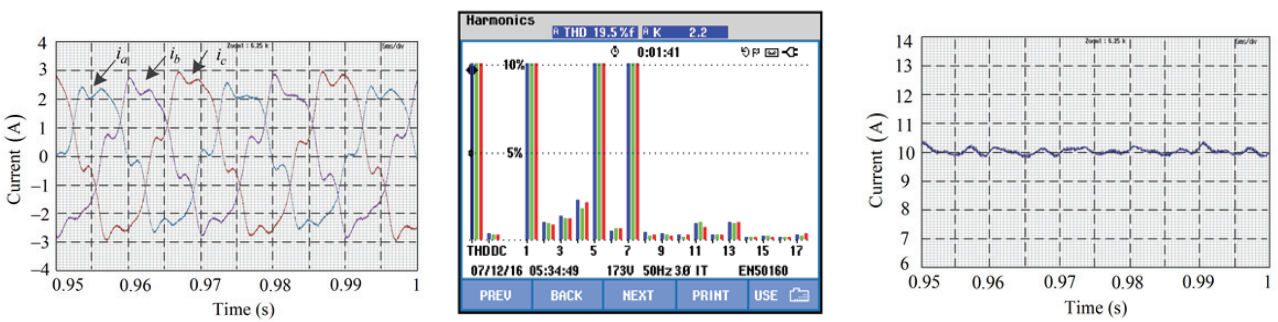

(a) (b) (c)

Fig. 18. Experimental waveforms of objective 3: (a) grid current; (b) spectrum diagram of the grid current; (c) DC-link current.

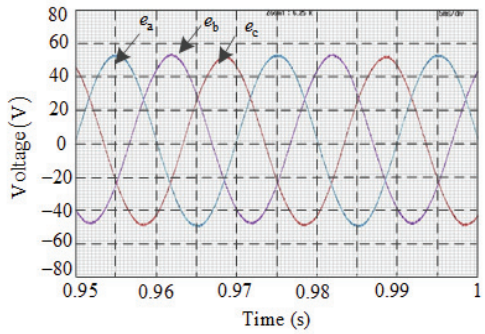

Fig. 19. Three-phase balanced grid voltage without harmonics.

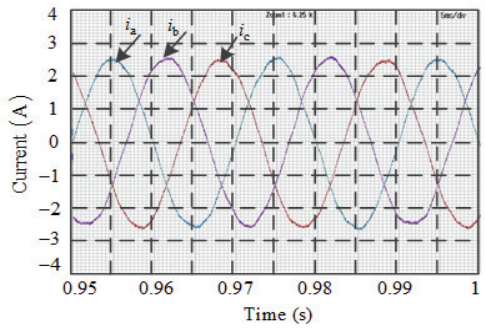

(a)

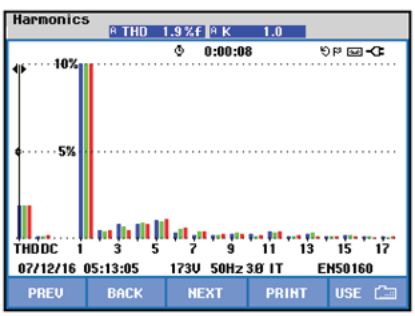

(b)

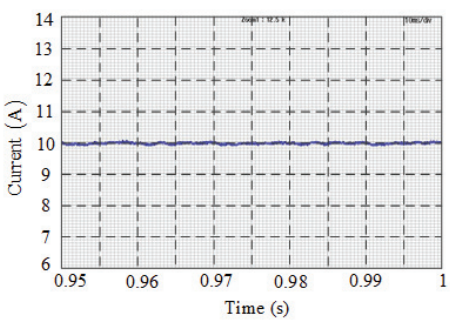

(c)

Fig. 20. Experimental waveform under a balanced grid voltage without harmonics: (a) grid current; (b) spectrum diagram of the grid current; (c) DC-link current.

When the proposed improved control with objective 3 is employed, as shown in Fig. 18, the fluctuation of the DC-link current is suppressed to ± 0.2A. In addition, the 2nd and 6th order fluctuations of the DC-link current are effectively suppressed. The THD is 19.5% and the imbalance degree is 5.4%. Furthermore, the negative-sequence components of the grid current are used to suppress the 2nd and 6th order fluctuations of the DC-link current. Therefore, the increases of the imbalance degree and distortion are consistent with the theory and the simulation results.

The above experimental results verify the validity of the proposed control strategy under unbalanced and harmonics grid voltage condition. Fig. 19 and Figs. 20 show experimental results under a balanced grid voltage without harmonics.

As shown in Fig. 20, the DC current is stable and the grid current is symmetrical and sinusoidal with a low THD of 1.9%. Thus, the proposed control strategy still works under a balanced grid voltage without harmonics.

VI. Conclusion

In this paper, a flexible multi-objective control strategy is proposed to control the DC-link and AC-link currents for a CSR under unbalanced and harmonic grid voltage conditions. A mathematical model of a CSR is established. In addition, the proposed control strategy is used to achieve three control objectives: 1) achieving a sinusoidal and symmetrical grid current; 2) achieving a sinusoidal grid current, and elimination of the DC-current 2nd order fluctuations; 3) elimination of the DC-current 2nd and 6th order fluctuations. Furthermore, it is not necessary to separate the components of the grid current for the proposed control strategy. Experimental results show that the proposed control strategy can enhance the performance of a CSR under unbalanced and harmonic grid voltage conditions. This can also be applied to a voltage-source PWM rectifier.

References

[1] J. Wu, Y. Liu, X. Li, M. Dong, and D. Guo, "Resonance Suppression method of current source active power based on instantaneous comparison control," *Transactions of China Electrotechnical Society*, Vol. 28, No. 9, pp. 73-78, Sep. 2013.

[2] K. Imaie, O. Tsukamoto, and Y. Nagai, "Control strategies for multiple parallel current-source converters of SMES system," *IEEE Trans. Power Electron.*, Vol. 15, No. 2, pp. 377-385, Mar. 2000.

[3] S. Kouro, J. Rodriguez, B. Wu, S. Bernet, and M. Perez, "Powering the future of industry high power adjustable speed drive topologies," *IEEE Ind. Appl. Mag.*, Vol. 18, No. 4, pp. 26-39, Jul./Aug. 2012.

[4] X. Guo, D. Xu and B. Wu, "Common-mode voltage mitigation for back-to-back current source converter with optimal space-vector modulation," *IEEE Trans. Power Electron.*, Vol.31, No. 1, pp. 688-697, Jan. 2016.

[5] S. Anand, S. K. Gundlapalli, and B. G. Fernandes, "Transformer-less grid feeding current source inverter for solar photovoltaic system," *IEEE Trans. Ind. Electron.*, Vol. 61, No. 10, pp. 5334-5344, Oct. 2014.

[6] Y. Xia, K. H. Ahmed, and B. W. Williams, "A PWM current

source-based DC transmission system for multiple wind turbine interfacing," *IEEE J. Emerg. Sel. Topics Power Electron.*, Vol. 2, No. 4, pp. 784-796, Dec. 2014.
[7] M. Wang, C. Xia, Z. Song, and T. Shi, "A power resonance compensation control strategy for PWM rectifiers under unbalanced grid voltage conditions," *Proc. Chin. Soc. Elec. Eng.*, Vol. 32, No. 21, pp. 46-53, Jul. 2012.
[8] Q. Cheng, Y. Cheng, H. Wang, X. Hu, and Y. Bai, "Development review of control methods for three phase current source PWM rectifiers," *East China Electric Power*, Vol. 41, No. 2, pp. 405-411, Feb. 2015.
[9] Y. Li and Z. Zhang, "Control strategy for current-source converter under unbalanced network voltage conditions," *Automation of Electric Power Systems*, Vol. 29, No. 16, pp. 72-75, Aug. 2005.
[10] Z. Wang, S. Fan, Z. Zou, Y. Huang, and M. Cheng, "Control strategies of current-source inverters for distributed generation under unbalanced grid conditions", in *IEEE Energy Conversion Congress and Exposition (ECCE)*, 2012, pp. 4671-4675.
[11] V. Vekhande, V. K. Kanakesh, and B. G. Fernandes, "Control of three-phase bidirectional current-source converter to inject balanced three-phase currents under unbalanced grid voltage condition," *IEEE Trans. Power Electron.*, Vol. 31, No. 9, pp. 6719-6737, Sep. 2016.
[12] S. Huang, L. Xiao, K. Huang, Z. Chen, and S. Xiong, "Operation and control on the grid-side converter of the directly-driven wind turbine with PM synchronous generator during asymmetrical faults," *Transactions of China Electrotechnical Society*, Vol. 26, No. 2, pp. 173-180, Feb. 2011.
[13] J. Kearney, M. F. Conlon, and E. Coyle, "The application of multi frequency resonant controllers in in a DFIG to improve performance by reducing unwanted power and torque pulsations and reducing current harmonics," in *the 45th International Universities Power Engineering Conference (UPEC)*, pp. 1-6, 2010.
[14] J. Wang, Y. Zhang, P. Cheng, and H. Nian, "Auxiliary control strategy of DFIG's GSC during network unbalance based on reduced-order resonant controller," *Transactions of China Electrotechnical Society*, Vol. 30, No. 4, pp. 35-43, Feb. 2015.
[15] H. Nian, P. Cheng, and Z. Q. Zhu, "Coordinated direct power control of DFIG system without phase-locked loop under unbalanced grid voltage conditions," *IEEE Trans. Power Electron.*, Vol. 31, No. 4, pp. 2905-2918, Apr. 2016.
[16] P. Cheng and H. Nian, "Collaborative control of DFIG system during network unbalance using reduced-order generalized integrators," *IEEE Trans. Energy Convers*., Vol. 30, No. 2, pp. 453-464, Jun. 2015.
[17] X. Guo, J. Li, X. Zhang, Z. Lu, B. Wang, and X. Sun, "Constant DC voltage control strategy for three-phase PWM rectifier without phase locked loop under distorted and unbalanced conditions," *Proc. Chin. Soc. Elec. Eng.*, Vol. 35, No. 8, pp. 2002-2008, Apr. 2015.
[18] J. B. Hu, W. Zhang, H. S. Wang, Y. H. He, and L. Xu, "Proportional integral plus multi-frequency resonant current controller for grid-connected voltage source converter under imbalanced and distorted supply voltage conditions," *Journal of Zhejiang University Science A*, Vol. 10, No. 10, pp. 1532-1540, Oct. 2009.
[19] H. Nian and Y. Quan, "Enhanced control technique of PWM converter under harmonically distorted voltage conditions," *Proc. Chin. Soc. Elec. Eng.*, Vol. 32, No. 9, pp. 41-48, Mar. 2012.
[20] J. Hu, H. Nian, H. Xu, and Y. He, "dynamic modeling and improved control of DFIG under distorted grid voltage conditions," *IEEE Trans. Energy Convers.*, Vol. 26, No. 1, pp. 163-175, Mar. 2011.
[21] H. Xu, J. Hu, and Y. He, "Integrated modeling and enhanced control of DFIG under unbalanced and distorted grid voltage conditions," *IEEE Trans. Energy Convers.*, Vol. 27, No. 3, pp. 725-736, Sep. 2012.
[22] P. Rodriguez, A. Luna, I. Etxeberria, J. R. Hermoso, and R. Teodorescu, "Multiple second order generalized integrators for harmonic synchronization of power converters," *IEEE Energy Conversion Congress and Exposition(ECCE)*, pp. 2239-2246, 2009.

Yi-Wen Geng was born in Jiangsu Province, China, in 1977. He received his B.S., M.S. and Ph.D. degrees from the School of Electrical and Power Engineering, China University of Mining and Technology, Xuzhou, China, in 2000, 2004 and 2014, respectively. From 2006 to 2016, he was a Lecturer in the School of Electrical and Power Engineering, China University of Mining and Technology. Since 2016, he has been with the Department of Electrical and Power Engineering, China University of Mining and Technology, where he is presently working as an Associate Professor. His current research interests include photovoltaic inverters, harmonic mitigation and power electronics.

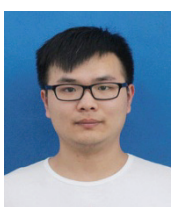

Hai-Wei Liu was born in Jiangsu Province, China, in 1994. He received his B.S. degree in Electrical Engineering from the China University of Mining and Technology, Xuzhou, China, in 2016, where he is presently working towards his M.S. degree in Electrical Engineering in the School of Electrical and Power Engineering. His current research interests include the control of current-source converters and ac machines.

Ren-Xiong Deng was born in Hunan Province, China, in 1992. He received his B.S. degree in Electrical Engineering from the China University of Mining and Technology, Xuzhou, China, in 2015, where he is presently working towards his M.S. degree in Electrical Engineering in the School of Electrical and Power Engineering. His current research interests include the control of current source inverters and photovoltaic generation technologies.

Fang-Fang Tian was born in Hebei Province, China, in 1990. She received her B.S. degree in Electrical Engineering from the China University of Mining and Technology, Xuzhou, China, in 2015, where she is presently working towards her M.S. degree in Electrical Engineering in the School of Electrical and Power Engineering. Her current research interests include the control of grid connected converters and harmonic mitigation.

Hao-Feng Bai was born in Heilongjiang, China, in 1989. He received his B.S. and M.S. degrees in Electric Engineering from the China University of Mining and Technology, Xuzhou, China, in 2011 and 2014, respectively. He is presently working towards his Ph.D. degree at Aalborg University, Aalborg, Denmark. His current research interests include the control of grid connected converters, power quality improvement and renewable power generation.

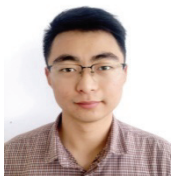

Kai Wang was born in Anhui, China, in 1992. He received his B.S. and M.S. degrees in Electric Engineering from the China University of Mining and Technology, Xuzhou, China, in 2014 and 2016, respectively, where he is presently working towards his Ph.D. degree in Electric Engineering in the School of Electrical and Power Engineering. His current research interests include the control of PWM converters, parallel converter systems and photovoltaic generation technologies.